

CLEO-c Hot Topics

R. Poling

University of Minnesota, 116 Church Street SE, Minneapolis, MN 55455

Selected recent results and future prospects for the CLEO-c experiment at CESR are reviewed. The topics covered include measurements of leptonic and semileptonic charm decays made with data collected at the $\psi(3770)$ resonance and results from a scan of the center-of-mass energy range from 3970 to 4260 MeV addressing the details of open-charm production and properties of the $Y(4260)$ state observed last year by BaBar.

1. Introduction

The CLEO-c experiment at the Cornell Electron Storage Ring (CESR) has provided our field with an unanticipated opportunity to turn the power of a state-of-the-art magnetic spectrometer developed for studying B decays to long-neglected problems of charm physics [1]. This paper is the first of several from CLEO-c in these proceedings, and includes a number of interesting early results from the CLEO-c charm program. Additional details and other topics are covered elsewhere in this volume in the papers of Cinabro, Stone, Vogel, and Wiss.

The remainder of this introduction provides an overview of the accelerator, detector, and motivation for CLEO-c. Sect. 2 describes results in leptonic and semileptonic D decays. Sect. 3 describes results on closed- and open-charm production in the center-of-mass energy range from 3970 to 4260 MeV from a scan completed in fall 2005. In Sect. 3 I provide a short summary and projection of what will come from CLEO-c before it concludes operation in 2008.

The CESR-c/CLEO-c project arose from the recognition that we had available to us a facility of great versatility that was no longer competitive for the job it was designed to do. The asymmetric B factories came on line with such excellent performance that it quickly became apparent that CESR and CLEO III could not perform at a comparable level. We recognized that we needed a niche that is complementary to Belle and BaBar. Plans were formulated in coordination with the CESR accelerator group to implement operations at about one-third of CESR's design energy, with charm physics as the principal objective. While conversion plans were being executed, we conducted productive runs on the narrow bottomonium resonances and made initial tests of $\psi(2S)$ operations.

By early 2004 the transformation was complete, and we had implemented Eq. 1:

$$\text{CESR} - c \simeq \text{CESR} - 6.5 \text{ GeV} + 12(\text{wigglers}), \quad (1)$$

where the superconducting wiggler magnets provide enhanced damping of the stored beams that is required because of the reduction of CESR's energy from ~ 10 GeV to ~ 4 GeV. The wigglers functioned well, but luminosity performance has fallen short of

expectations. Various problems have been uncovered, and many improvements implemented, including enhanced instrumentation in the form of a fast-feedback luminosity monitor. With more detailed measurements and an extensive simulation program, it was determined that specific-luminosity limitations were partially due to energy sensitivity in the compensation for CLEO's solenoidal magnetic field. This led to several optics and operational changes for CESR, in particular a new "antisolenoid" magnet modeled on a similar compensation scheme devised at Frascati. It was installed in January, 2006 and the benefits when running resumed were immediate, with an initial $\sim 20\%$ improvement in instantaneous luminosity (to $6.7 \times 10^{31} \text{ cm}^{-2}\text{s}^{-1}$) and in "best-day" integrated luminosity (to $\sim 4.2 \text{ pb}^{-1}$). Machine studies aimed at achieving the full benefit of the antisolenoid and other improvements continue, and we expect to collect at least 5 pb^{-1} per day in coming runs.

In preparing for the new energy regime, only modest modifications were needed for CLEO's detector (Fig. 1), as described in Eq. 2:

$$\text{CLEO} - c \simeq \text{CLEO III} - \text{SVX} + \text{ZD} - 0.5 \text{ T}, \quad (2)$$

where the previous silicon vertex detector (SVX) was replaced by a low-mass all-stereo drift chamber (ZD) and the magnetic field was reduced to mitigate the effect of soft particles curling up in the tracking volume.

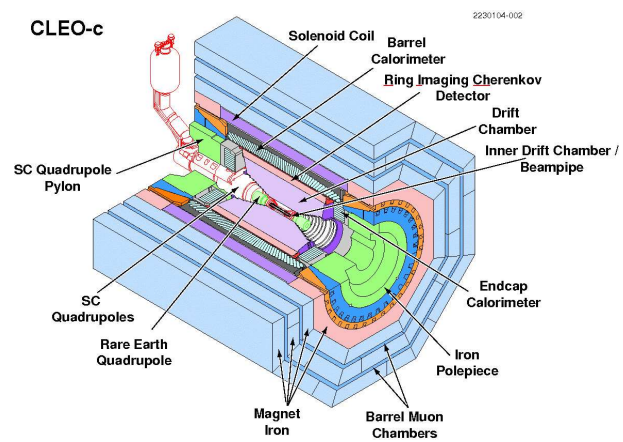


Figure 1: CLEO-c detector.

The conversion to CLEO-c has been a great success, and the detector remains at the top of its game, with charged-particle momentum resolution ($\Delta p/p = 0.6\%$ at 1 GeV/ c) and electromagnetic calorimetry ($\Delta E/E = 2.2\%$ at 1 GeV and 5% at 100 MeV) superior to other detectors that have operated near charm threshold. Excellent electron identification and hadron identification (RICH and dE/dx) are likewise unprecedented tools for charm physics in this energy range.

The opportunity that CLEO-c represented at the time of its proposal is now being realized, in spite of the reduction by roughly a factor of 4 in expected integrated luminosity. Impact on the worldwide CKM program is both direct and indirect, and will be leveraged powerfully in the interpretation of B decays through precision tests of theoretical tools like lattice QCD. In addition, “engineering” input such as branching fractions for key normalization modes in D and D_s decays will be crucial.

The data samples that have been used for the results presented in this paper include a total of 281 pb^{-1} collected at the $\psi(3770)$ resonance. Many initial results from the first 57 pb^{-1} of this sample have been published, and initial results from the full sample have begun to appear, including several that are new for FPCP 2006. The D_s scan run consisted of a total of about 60 pb^{-1} at twelve energy points above the $\psi(3770)$, and it immediately led to CLEO-c’s first dedicated D_s run at 4170 MeV, which was completed in April, 2006. There has also been a small amount of data collected at the $\psi(2S)$ resonance, split equally between CLEO III and CLEO-c. While totaling only 5.6 pb^{-1} , this sample has produced 40 analysis results, some of which are described elsewhere in these proceedings.

2. D Physics at $\psi(3770)$: Leptonic and Semileptonic

Much of the progress in heavy-flavor physics has come through detailed studies of leptonic and semileptonic decays. In B physics we use events with leptons to gain access to unknown Standard Model parameters with less uncertainty due to strong-interaction effects than in purely hadronic decays. As experimental precision has improved, however, essentially every determination of CKM parameters, especially of the magnitudes $|V_{cb}|$ and $|V_{ub}|$, has become systematic-limited by theoretical uncertainties. Studies of charm semileptonic and leptonic decays complement B -decay measurements by providing an opportunity to master hadronic effects. Heavy-quark symmetry predicts relationships between processes involving c quarks and those involving b quarks in very general ways, and specific theoretical tools like lattice QCD (LQCD) can be used to leverage knowledge gleaned from charm into precise predictions about B .

In leptonic decays the hadronic effects are packaged in the decay constant (f_{D^+} , f_{D_s}), as shown in Eq. 3.

$$\Gamma(D^+ \rightarrow \ell^+ \nu) = \frac{G_F^2}{8\pi} f_{D^+}^2 m_\ell^2 M_{D^+} \left[1 - \frac{m_\ell^2}{M_{D^+}^2} \right]^2 |V_{cd}|^2 \quad (3)$$

Precise tests of LQCD are possible through measurements of leptonic D^+ and D_s^+ decay constants (or, even more precisely, their ratio). Calculations of the corresponding quantities for B_d and B_s decays then can be used to reduce the theoretical uncertainties in extracting CKM parameters from measurements of B_d and B_s mixing. In exclusive semileptonic decays the hadronic effects are bundled in the form factors, as shown for D to pseudoscalar transitions in Eq. 4.

$$\Gamma(D \rightarrow P \ell \nu) = \frac{G_F^2 |V_{cq}|^2 p^3}{24\pi^3} |f_+(q^2)|^2 \quad (4)$$

As with much of the CLEO-c charm program, most measurements of leptonic and semileptonic decays rely on tagging one of the D mesons in the pure $D\bar{D}$ state produced in $\psi(3770)$ decays. Full reconstruction of a D meson on one side of tagged events effectively provides a “beam” of D ’s of known 4-momentum on the other side. Depending on the cleanliness of the process being measured, the selection of tags can be fine-tuned, with low-multiplicity “golden modes” for best purity and additional modes with higher charged multiplicity and/or π^0 ’s for best efficiency. Typical tagging efficiencies in CLEO-c analyses are in the range of 15% for D^0 and 10% for D^+ .

A 2004 measurement of the leptonic decay $D^+ \rightarrow \mu^+ \nu_\mu$ was the first CLEO-c result to be presented, and a follow-up measurement with the current full $\psi(3770)$ data sample of 281 pb^{-1} has been published [2]. A total of about 160,000 D^+ tags are selected in six hadronic decay modes. Signal events are required to have a tag accompanied by exactly one track of charge opposite to the tag, with minimal extra energy in the event. The track is required to have a muon-like energy deposit of less than 300 MeV in the electromagnetic calorimeter. True $D^+ \rightarrow \mu^+ \nu_\mu$ decays are selected based on the missing-mass-squared variable MM^2 defined in Eq. 5.

$$\text{MM}^2 = (E_{beam} - E_{\mu^+})^2 - (-\mathbf{p}_{D^-} - \mathbf{p}_{\mu^+})^2 \quad (5)$$

The MM^2 distribution in the data is shown in Fig. 2. There is a clear signal in the vicinity of $\text{MM}^2 = 0$, cleanly separated from the potentially severe background of $D^+ \rightarrow K_L^0 \pi^+$. Potential backgrounds at low MM^2 , like $D^+ \rightarrow \pi^0 \pi^+$ are effectively suppressed by the extra-energy cut. Overall, there are 50 events in the $D^+ \rightarrow \mu^+ \nu_\mu$ signal region, with a total background of 2.81, where we use data as much as possible to estimate the larger background sources. This leads to the following branching fraction measurement:

$$\mathcal{B}(D^+ \rightarrow \mu^+ \nu_\mu) = (4.4 \pm 0.7 \pm 0.1 \times 10^{-4}), \quad (6)$$

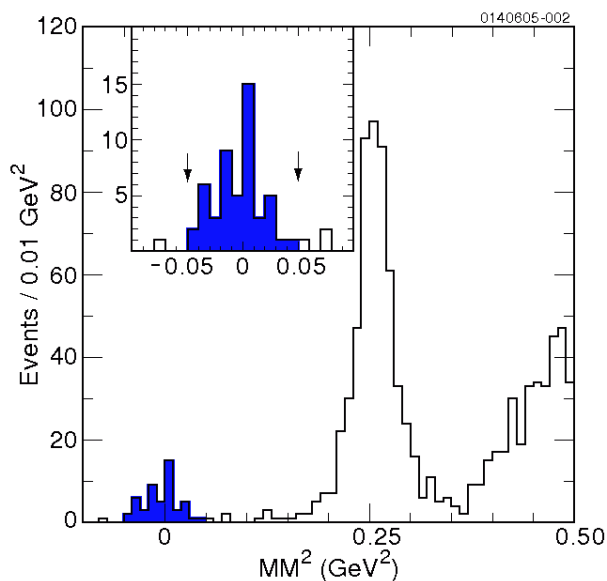


Figure 2: MM^2 for events with selected D^- tags, an oppositely-charged muon-like track, and minimal extra energy. The inset shows a close-up of the signal region, with cut values indicated by the arrows.

and a value for the decay constant of

$$f_{D^+} = (223 \pm 17 \pm 3) \text{ MeV}. \quad (7)$$

This result is consistent with the LQCD prediction of Aubin *et al.* [3] of $(201 \pm 3 \pm 17) \text{ MeV}$. The juxtaposition of the experimental and theoretical statistical and systematic uncertainties illustrates that, with more data from CLEO-c, there is an excellent opportunity to put the lattice to a rigorous test.

The CLEO-c program of leptonic-decay studies aspires to measure all accessible modes with the best precision possible to verify internal consistency and check for conformance to Standard Model expectations. In this context, Ref. [2] includes a limit on the branching fraction for $D^+ \rightarrow e^+\nu_e$, applying exactly the same selection procedures except that the single candidate track is required to pass an electron-identification requirement. The 90% confidence level upper limit for $D^+ \rightarrow e^+\nu_e$ of 2.3×10^{-5} is well above the Standard Model prediction, which is smaller than that for the muon mode by a factor of 50,000.

In the same vein, CLEO-c has recently submitted to Phys. Rev. D a search for the leptonic decay $D^+ \rightarrow \tau^+\nu_\tau$ [4]. This provides complementary information to $D^+ \rightarrow \mu^+\nu_\mu$ and potential further verification that leptonic charm decays present a picture consistent with the Standard Model. The decay $D^+ \rightarrow \tau^+\nu_\tau$ has a much smaller helicity suppression than $D^+ \rightarrow \mu^+\nu_\mu$ because of the large mass of the τ compared to the μ . This is partially defeated by limited phase space, however, so that the expected advantage in branching fraction is only a factor of

2.65. The limited phase space is also the reason that $D^+ \rightarrow \tau^+\nu_\tau$ can be measured with a technique that is only a slight modification of that for $D^+ \rightarrow \mu^+\nu_\mu$, with identical tag selection and procedures for extracting signal yields and estimating background. The candidates are divided into subsamples that are either muon-like (calorimeter energy less than 300 MeV) or not (calorimeter energy greater than 300 MeV - rare for muons, less so for pions). The presence of the extra neutrino from the τ decay produces a distribution in MM^2 , rather than the narrow peak of the $D^+ \rightarrow \mu^+\nu_\mu$. The slowness of the τ keeps MM^2 values low, however, populating the region between the $D^+ \rightarrow \mu^+\nu_\mu$ and $D^+ \rightarrow K_L^0\pi^+$. Subdividing the sample increases the efficiency of the selection, since for pion-like tracks we can include the $MM^2 = 0$ region in the signal. The MM^2 distributions are shown in Fig. 3. For the $p < 300 \text{ MeV}$ ($p > 300 \text{ MeV}$) sample there are 12 (8) candidates with an estimated background of $6.1 \pm 0.6 \pm 0.3$ ($5.0 \pm 0.6 \pm 0.2$), giving a net yield of $5.9 \pm 3.5 \pm 0.3$ ($3.0 \pm 2.9 \pm 0.2$). In neither

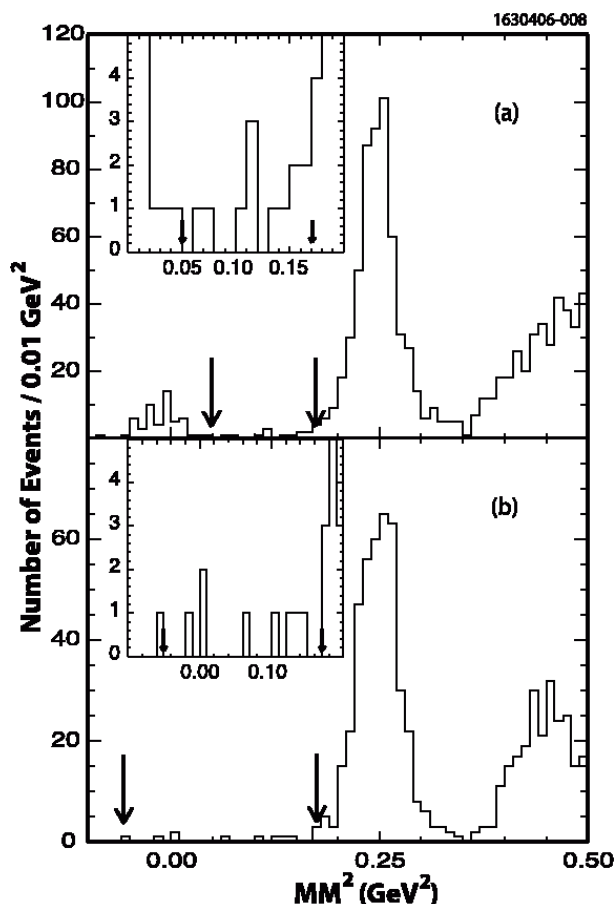


Figure 3: MM^2 for events with selected D^- tags, an oppositely-charged track with (a) $p < 300 \text{ MeV}$ or (b) $p > 300 \text{ MeV}$, and minimal extra energy. The limits of the $D^+ \rightarrow \tau^+\nu_\tau$ signal regions in the two cases are indicated by the arrows.

case is there a statistically significant excess, and the resulting upper limit is

$$\mathcal{B}(D^+ \rightarrow \tau^+ \nu_\tau) < 2.1 \times 10^{-4} \text{ (90\% confidence)}. \quad (8)$$

This does not yet constitute a rigorous test of the Standard Model prediction, which is larger than this limit by a factor of 1.8.

In the realm of semileptonic charm decays CLEO-c has both inclusive and exclusive analyses presented and forthcoming that represent significant advances beyond previous knowledge. Inclusive decays $D \rightarrow Xe^+ \nu_e$ are of interest as a cross-check of exclusive measurements, to determine whether the apparent saturation by the lightest vector and pseudoscalar modes survives to higher precision or if there is significant room for as-yet-unobserved exclusive modes. Comparisons of the charged and neutral semileptonic widths probe for contributions other than tree-level diagrams, such as the weak-annihilation processes that constitute a possible background for charmless semileptonic B decays [5]. Finally, the inclusive measurements are important input for other experiments, which need the branching fractions and momentum spectra for precise modeling of secondary charm decays in B studies. CLEO-c has recently presented measurements of inclusive D^0 and D^+ semileptonic decays based on the $281 \text{ pb}^{-1} \psi(3770)$ sample [6]. This analysis uses only the purest tags, roughly 47,000 $D^0 \rightarrow K^- \pi^+$ (signal/background ~ 60) and 74,000 $D^+ \rightarrow K^- \pi^+ \pi^-$ (S/B ~ 25). Electrons are measured with a minimum-momentum requirement of $200 \text{ MeV}/c$, giving access to about 92% of the full spectrum. The solid-angle acceptance of 80% of 4π corresponds to the fiducial volume of the RICH detector. The electron-identification efficiency, determined with data, is about 95% above $300 \text{ MeV}/c$ and about 71% between 200 and $300 \text{ MeV}/c$. The probability of misidentifying a charged hadron as an electron, also determined with data, is about 0.1% over most of the momentum range. We rely on charge correlations to eliminate charge-symmetric electron backgrounds due to photon conversions and π^0 Dalitz decays. The yield measurement is summarized in Table I, and the lab-frame momentum spectra for semileptonic D^+ and D^0 decays are shown in Fig. 4. D -frame spectra will be presented in a forthcoming publication. There is good agreement between the spectra for charged and neutral D 's, and both are fitted to theoretical models that include final-state radiation to determine the correction for the unmeasured portion of the spectra. The resulting branching fraction measurements are given in Eqs. 9 and 10.

$$\mathcal{B}(D^+ \rightarrow Xe^+ \nu_e) = (16.13 \pm 0.20_{\text{stat}} \pm 0.33_{\text{sys}})\% \quad (9)$$

$$\mathcal{B}(D^0 \rightarrow Xe^+ \nu_e) = (6.46 \pm 0.17_{\text{stat}} \pm 0.13_{\text{sys}})\% \quad (10)$$

Table I Positron unfolding procedure and corrections for the inclusive D semileptonic measurements. The errors reported in the intermediate yields reflect only statistical uncertainties.

| | D^+ | D^0 |
|-----------------------|-----------------|---------------|
| Signal e^+ | | |
| Right-sign (raw) | 8275 ± 91 | 2239 ± 47 |
| Wrong-sign (raw) | 228 ± 15 | 233 ± 15 |
| Right-sign (unfolded) | 9186 ± 103 | 2453 ± 54 |
| Wrong-sign (unfolded) | 231 ± 19 | 203 ± 19 |
| Sideband e^+ (RS) | 168 ± 13 | 15 ± 4 |
| Sideband e^+ (WS) | 11 ± 5 | 11 ± 4 |
| Net e^+ | 8798 ± 105 | 2246 ± 57 |
| Corrected Net e^+ | 10998 ± 132 | 2827 ± 72 |

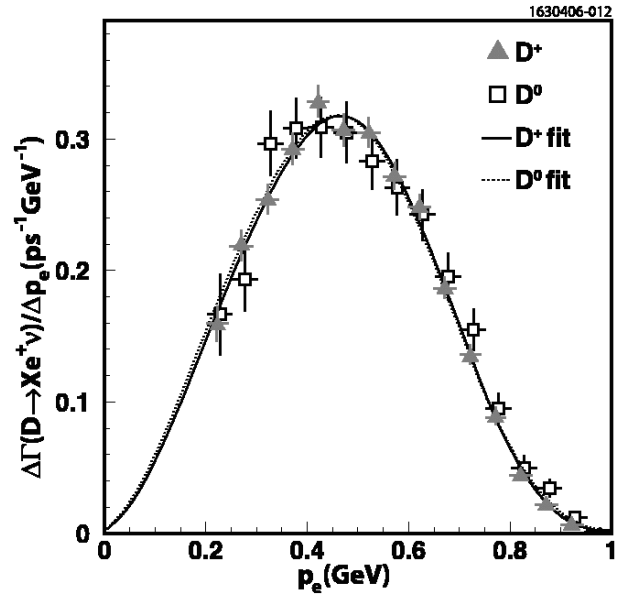


Figure 4: Positron differential semileptonic widths $d\Gamma^{\text{sl}}/dp_e$ for the decays $D^+ \rightarrow Xe^+ \nu_e$ (filled triangles) and $D^0 \rightarrow Xe^+ \nu_e$ (open squares) in the laboratory frame. The errors shown include statistical errors and additive systematic errors. The symbols for D^+ and D^0 spectra are shifted for clarity. The curves represent the fits to extrapolate the measured spectra below $200 \text{ MeV}/c$.

Combining these branching fractions with measurements of D lifetimes [7] gives values for the total inclusive semileptonic widths of $\Gamma(D^+ \rightarrow Xe^+ \nu_e) = 0.1551 \pm 0.0020 \pm 0.0031 \text{ ps}^{-1}$ and $\Gamma(D^0 \rightarrow Xe^+ \nu_e) = 0.1574 \pm 0.0041 \pm 0.0032 \text{ ps}^{-1}$. Their ratio, $\Gamma_{D^+}^{\text{sl}}/\Gamma_{D^0}^{\text{sl}} = 0.985 \pm 0.028 \pm 0.015$, is consistent with the expectation of isospin invariance.

CLEO-c has previously published measurements of the branching fractions for five D^+ [8] and five D^0 [9] exclusive semileptonic modes based on the first 57 pb^{-1} of $\psi(3770)$ data. In every case these are

improvements over previous world averages [7], and two of the modes ($D^+ \rightarrow \omega e^+ \nu_e$ and $D^0 \rightarrow \rho^- e^+ \nu_e$) are first measurements. Extensions of this exclusive semileptonic study to 281 pb^{-1} , including additional modes and form-factor measurements, are in progress. Results are expected in summer 2006.

A new preliminary CLEO-c analysis takes an alternative approach to measuring the branching fractions and form factors for the exclusive decays $D \rightarrow P e \nu$, where P signifies a pseudoscalar (π or K). In this case there is no D -tag requirement, but rather full reconstruction of the semileptonic decay from all decay products, including the neutrino. The technology of “neutrino reconstruction” was developed for CLEO II initially for exclusive $b \rightarrow u \ell \nu$ measurements. The measured missing momentum and energy in the event are assigned to the neutrino: $P_\nu \equiv P_{\text{event}} - P_{\text{visible}}$, allowing computation of the event ΔE , M_{bc} , and q^2 . Special track- and shower-selection criteria ensure, to the maximum extent possible, that all true particles are included, with no false ones or duplicates. To make this feasible, events are chosen selectively: no net charge and only one identified lepton, since a second lepton signals the presence of a second neutrino.

This procedure yields one-sigma resolution in the core of the measured P_{miss} distribution of $\sim 13 \text{ MeV}$. The resolution in the missing energy is significantly poorer, so the measured missing energy is replaced by the magnitude of the missing momentum. In computing M_{bc} and q^2 , the resolution is improved by scaling the 4-momentum to satisfy $\Delta E=0$.

Semileptonic decay candidates are selected by cutting on ΔE and fitting M_{bc} distributions. This is done in five bins in q^2 and the resulting $d\mathcal{B}/dq^2$ distributions can be integrated to get the branching fractions and fitted to obtain the form-factor parameters. M_{bc} fits summed over all q^2 bins for all four $D \rightarrow P e \nu$ modes are shown in Fig. 5. The signals are clear and the fits, which include backgrounds from data and simulations, are excellent. The resulting branching fractions are as follows:

$$\mathcal{B}(D^0 \rightarrow K^- e^+ \nu_e) = (3.56 \pm 0.03 \pm 0.10)\% \quad (11)$$

$$\mathcal{B}(D^0 \rightarrow \pi^- e^+ \nu_e) = (0.301 \pm 0.011 \pm 0.010)\% \quad (12)$$

$$\mathcal{B}(D^+ \rightarrow K^0 e^+ \nu_e) = (8.70 \pm 0.13 \pm 0.27)\% \quad (13)$$

$$\mathcal{B}(D^+ \rightarrow \pi^0 e^+ \nu_e) = (0.381 \pm 0.025 \pm 0.015)\% \quad (14)$$

The ratios of branching fractions and partial widths are found to be $\mathcal{B}(D^0 \rightarrow \pi^- e^+ \nu)/\mathcal{B}(D^0 \rightarrow K^- e^+ \nu) = 0.085 \pm 0.003 \pm 0.001$, $\mathcal{B}(D^+ \rightarrow \pi^0 e^+ \nu)/\mathcal{B}(D^+ \rightarrow \bar{K}^0 e^+ \nu) = 0.044 \pm 0.003 \pm 0.001$, $\Gamma(D^0 \rightarrow \pi^- e^+ \nu)/\Gamma(D^+ \rightarrow \pi^0 e^+ \nu) = 2.04 \pm 0.15 \pm 0.08$, and $\Gamma(D^0 \rightarrow K^- e^+ \nu)/\Gamma(D^+ \rightarrow \bar{K}^0 e^+ \nu) = 1.06 \pm 0.02 \pm 0.03$. The

partial-width ratios are consistent with isospin symmetry.

The results of the fits for the form-factor parameters to the measured q^2 distributions with the simple pole [10] and the modified pole [11] models are given in Table II. The q^2 fits yield values of the inter-

| <i>Simple Pole Model</i> | | |
|-------------------------------------|-----------------------------|--------------------------|
| <i>Decay Mode</i> | $ V_{cx} f^+(0)$ | m_{pole} |
| $D^0 \rightarrow \pi^- e^+ \nu$ | $0.146 \pm 0.004 \pm 0.003$ | $1.87 \pm 0.03 \pm 0.01$ |
| $D^0 \rightarrow K^- e^+ \nu$ | $0.736 \pm 0.005 \pm 0.010$ | $1.98 \pm 0.03 \pm 0.02$ |
| $D^+ \rightarrow \pi^0 e^+ \nu$ | $0.152 \pm 0.007 \pm 0.004$ | $1.97 \pm 0.07 \pm 0.02$ |
| $D^+ \rightarrow \bar{K}^0 e^+ \nu$ | $0.719 \pm 0.009 \pm 0.012$ | $1.97 \pm 0.05 \pm 0.02$ |
| <i>Modified Pole Model</i> | | |
| <i>Decay Mode</i> | $ V_{cx} f^+(0)$ | α |
| $D^0 \rightarrow \pi^- e^+ \nu$ | $0.142 \pm 0.005 \pm 0.003$ | $0.37 \pm 0.09 \pm 0.03$ |
| $D^0 \rightarrow K^- e^+ \nu$ | $0.734 \pm 0.006 \pm 0.010$ | $0.19 \pm 0.05 \pm 0.03$ |
| $D^+ \rightarrow \pi^0 e^+ \nu$ | $0.151 \pm 0.008 \pm 0.004$ | $0.12 \pm 0.17 \pm 0.05$ |
| $D^+ \rightarrow \bar{K}^0 e^+ \nu$ | $0.718 \pm 0.009 \pm 0.012$ | $0.20 \pm 0.08 \pm 0.04$ |

Table II Simple-pole model and modified-pole model form-factor parameters resulting from fits to the $d\mathcal{B}/dq^2$ distributions for the four $D \rightarrow P e \nu$ decay modes.

cepts at $q^2=0$ which are equal to $|V_{cx}|f(0)$. These can be combined with LQCD calculations of $f(0)$ [12] to obtain preliminary results for the magnitudes of the CKM matrix elements which are consistent with current world averages, but are limited in precision by $\sim 10\%$ theoretical uncertainties.

The precision of the semileptonic measurements made by the neutrino-reconstruction is competitive with the tagged results. Because the techniques are so different, there is considerable statistical independence and the best CLEO-c results will come from averaging the two techniques.

3. The CLEO-c D_s Scan

When the CLEO-c program was proposed [1] its centerpiece was charm: direct and indirect CKM measurements, theoretical tests, and branching fractions and charm properties as engineering input for other experiments. Within the charm program there were two components: D^0 and D^+ leptonic, semileptonic and hadronic decays at the $\psi(3770)$ resonance, and D_s leptonic, semileptonic and hadronic decays at some energy to be determined. The mechanism for determining that energy was a two-month scan run that was carried out in late summer and early fall of 2005.

The principal goal of the scan was determination of the optimal energy for studying D_s physics. That optimum depends both on the production cross section and the complexity of the events that dominate

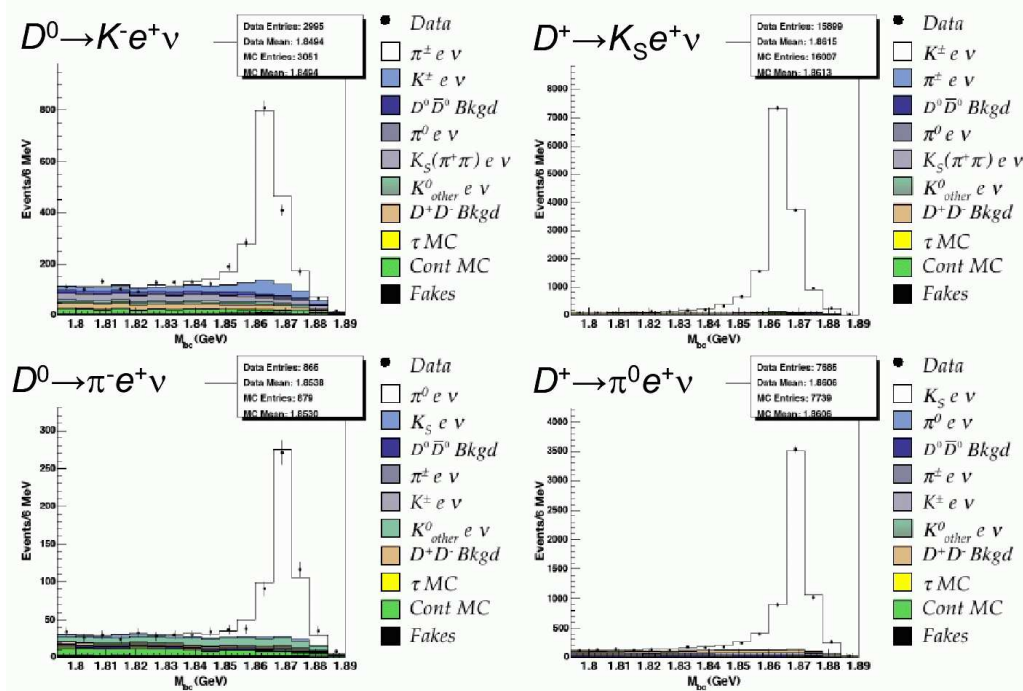


Figure 5: Fits to M_{bc} distributions for all four $D \rightarrow Pe\nu$ modes summed over all q^2 bins.

D_s production. This had to be measured by CLEO-c because, while there is beautiful data on hadron production in the region of charm threshold (Fig. 6) [7], there is little experimental detail on its composition and theoretical guidance is limited. Secondary motivations for the scan included assessing our ability to do

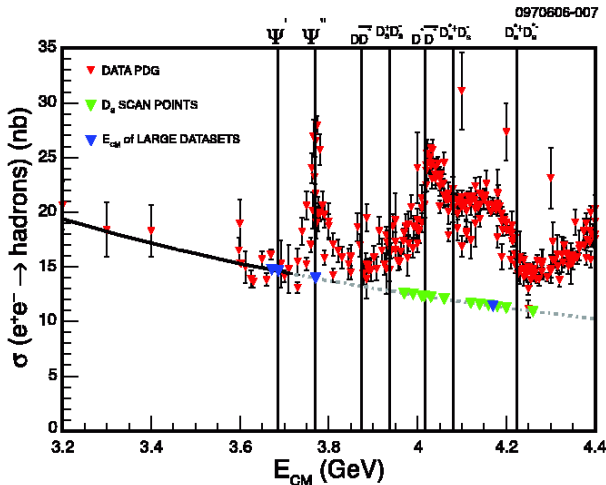


Figure 6: Data on hadron production (R) as a function of e^+e^- center-of-mass energy. Inverted green triangles indicate energies of the CLEO-c scan-run points and inverted blue triangles denote larger data samples at $\psi(2S)$, $\psi(3770)$, and $E_{CM} = 4170$ MeV, the last collected after the scan run. Prominent charmonium states and threshold energies for open-charm final states are indicated.

D^+ and D^0 physics at energies above $\psi(3770)$, disentangling the “intricate behavior” of charm production in the region above charm threshold [13], and confirming and investigating the $Y(4260)$ state discovered by BaBar last year [14].

The scan that was conducted consisted of twelve points in the energy region 3970-4260 MeV, totaling about 60 pb^{-1} . At each energy point the first task was to make quick determinations of the cross sections for each of the two-charmed-meson final states ($D_{(s)}^{(*)} \bar{D}_{(s)}^{(*)}$) that were accessible at that energy. This can be done cleanly and efficiently without attempting full reconstruction of D^* states by selecting D and D_s mesons with the usual tools of D tagging. Three, five and eight decay modes were employed for D^0 , D^+ and D_s^+ , respectively. The different production channels can be distinguished based on the kinematics of reconstructed tags reflected through the selection variables ΔE and M_{bc} , the latter of which is equivalent to $D_{(s)}$ momentum. Fig. 7 shows a two-dimensional plot of ΔE vs. M_{bc} for $D_s \rightarrow \phi\pi$ candidates from a Monte Carlo sample generated at 4160 MeV. There are clear concentrations of events at characteristic values. The $D_s^+ D_s^-$ appears as a tight cluster at $\Delta E=0$ and $M_{bc}=M_{D_s}$, for example, while the $D_s^+ D_s^{*-}$ is an elliptical structure with a central core consisting of direct D_s and smeared wings with D_s from D_s^* . Because of Cabibbo-suppressed modes that can populate this final state, there are also clusters for non-strange charmed-meson final states: $D\bar{D}$, $D\bar{D}^*$ and $D^* \bar{D}^*$.

The yields for $D\bar{D}$ and $D_s \bar{D}_s$ were extracted by

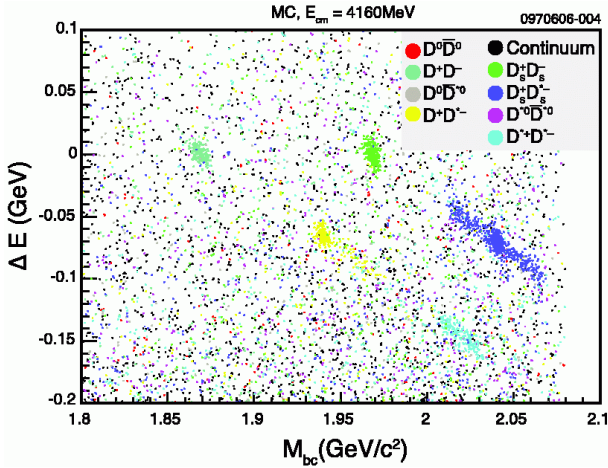


Figure 7: ΔE vs. M_{bc} for selected $D_s^+ \rightarrow \phi\pi^+$ candidates for Monte Carlo generated at $E_{CM} = 4160$ MeV. There is clear separation of candidates into different event types.

cutting on ΔE and projecting M_{bc} distributions. For the other event types the procedure was to cut on M_{bc} and project onto invariant mass to extract the yields. All cut values were determined by kinematics, with no double counting allowed. Cross-feed among modes is small and easily determined.

One complication that quickly became apparent from recoil-mass and charmed-meson momentum distributions is that two-body modes do not account for all charmed-meson production. There is clear evidence for “multibody” production such as $e^+e^- \rightarrow D\bar{D}^*\pi$. Work to thoroughly disentangle and account for this production mechanism is under way.

Preliminary cross-section results (partially evaluated systematic uncertainties, no correction for multibody contributions, not radiatively corrected) for the non-strange charmed meson combinations are shown in Fig. 8. There is very little $D\bar{D}$ production at any energy, a sharp peak structure in $D\bar{D}^*$ near $D^*\bar{D}^*$ threshold, and a broad peak or plateau in $D^*\bar{D}^*$. The charm cross section through this region is considerable, comparable to that at the $\psi(3770)$.

The corresponding (preliminary) bottom line for D_s production is shown in Fig. 9. In this case there is a visible, but disappointingly small, peak in $D_s\bar{D}_s$, and a more impressive broad peak at about 4170 MeV which offers about 1 nb of D_s production.

Many cross-checks of these results are being carried out. A straightforward one (Fig. 10) is a comparison of the exclusive measurements described so far with two inclusive measurements of charm production. One of these is the sum of the inclusive cross sections for D^0 , D^+ , and D_s^+ production and the second is a measurement of the total hadronic cross section with the extrapolated uds continuum subtracted based on lower-energy measurements. There is very good agreement between the two inclusive measurements, which

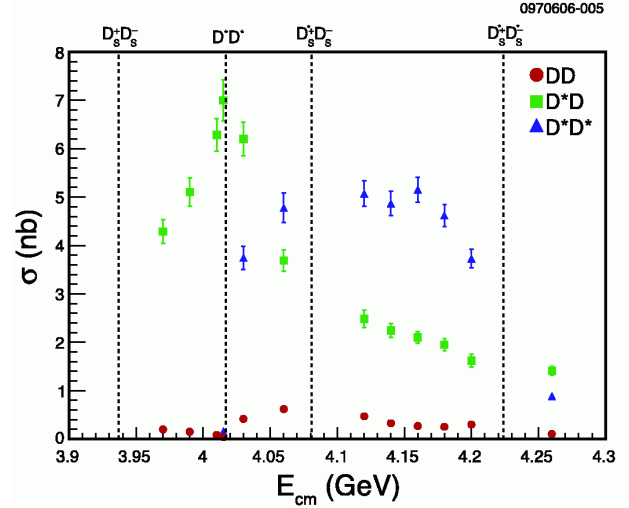


Figure 8: Cross sections for $D\bar{D}$, $D\bar{D}^*$, and $D^*\bar{D}^*$ from the CLEO-c scan run.

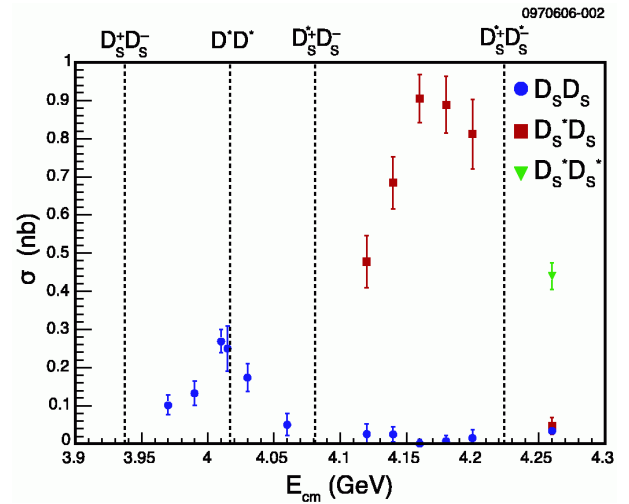


Figure 9: Cross sections for $D_s\bar{D}_s$, $D_s\bar{D}_s^*$, and $D_s^*\bar{D}_s^*$ (only accessible at the highest point) from the CLEO-c scan run.

exceed the exclusive by an amount that grows with energy. This is reaffirmation of the presence in the inclusive of something that is not (effectively) counted in the exclusive: multibody production.

Overall the scan was a great success for its primary purpose. It succeeded in identifying a D_s “mini-factory” at $E_{CM}=4170$ MeV which has already been used to acquire a sizable D_s sample. The roughly 1-nb cross-section measurement is dependent on the input branching fractions for the eight D_s selection modes. Refinement awaits the finalized D_s branching fractions from application of the single-tag/double-tag technique to CLEO-c 4170-MeV data.

The successful and early achievement of the core goals of the scan left us running time for two additions to the original program. The first was more running in the D_s peak-production region, providing a head start

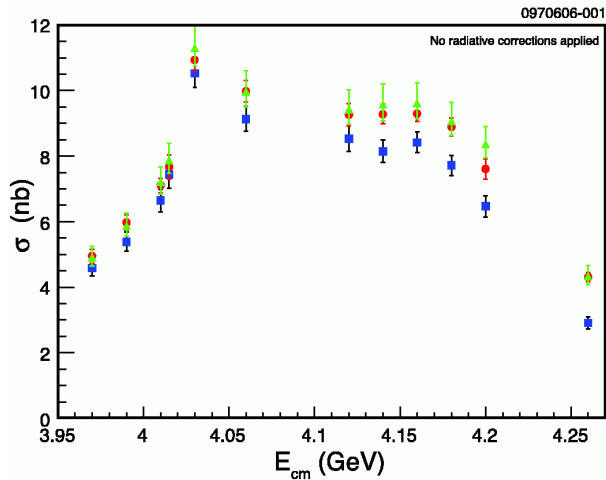


Figure 10: Cross sections for (blue) exclusive-charm measurement obtained by summing two-charmed-meson final states and two inclusive measurements: (red) straightforward inclusive counting of D^0 , D^+ and D_s cross sections, and (green) the total inclusive hadronic cross section minus the extrapolated uds continuum.

on the accumulation of a CLEO-c 4170-MeV sample which already amounts to about 200 pb^{-1} , and which is expected to grow to about twice that in summer 2006. The second addition was 13.2 pb^{-1} at $E_{cm} = 4260 \text{ MeV}$, primarily to investigate the $Y(4260)$.

BaBar's discovery of $Y(4260)$ [14] was based on a sample of 233 fb^{-1} collected at the $\Upsilon(4S)$. The observation of an enhancement in initial-state radiation (ISR) events of the form $e^+e^- \rightarrow \gamma(\pi^+\pi^-J/\psi)$ with effective energy 4260 MeV was unexpected, especially since that energy corresponds to a minimum in the cross section for $e^+e^- \rightarrow$ hadrons. Independent evidence supporting this discovery is accumulating, and there is now a preliminary observation of exactly the same mechanism in CLEO III data. The CLEO III observation (Fig. 11) is based on 13.3 fb^{-1} collected in the $\Upsilon(1S) - \Upsilon(4S)$ energy range. The statistical significance is 4.9σ , and the measurements of energy of $(4283^{+17}_{-16} \pm 5) \text{ MeV}$ and width of $(70^{+40}_{-25} \pm 4) \text{ MeV}$ are consistent with BaBar, although less precise.

There is a wide range of proposed explanations of the $Y(4260)$, including some that are highly speculative. They include hybrids, tetraquarks, molecular states, baryonium, and conventional charmonium with quantum mechanical complications. Clearly more information was needed, and since the original observation in ISR demonstrates an assignment of $J^{PC} = 1^{--}$, a search for direct production in e^+e^- annihilation by CLEO-c was a natural next step. Readiness for this study was excellent, since this process is closely related to others that have already been investigated in $\psi(2S)$ and $\psi(3770)$ data. The CLEO-c analysis [15] is a search for $Y(4260)$ in sixteen possible final states with J/ψ , $\psi(2S)$, χ_{cJ} ,

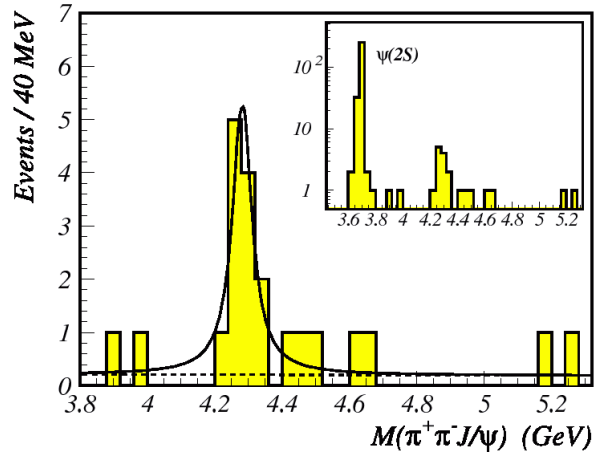


Figure 11: Fit to the $\pi^+\pi^-J/\psi$ mass distribution (with $J/\psi \rightarrow e^+e^-$, or $\mu^+\mu^-$) in CLEO III ISR events. The dotted line represents the fitted background and the solid curve the total fit. The inset (semilog) shows the same mass distribution over an extended range, allowing comparison with $\psi(2S)$.

and ϕ . It is summarized in Fig. 12. This analysis benefits from the availability of the ISR process $e^+e^- \rightarrow \gamma\psi(2S)$, which allows verification of the efficiencies, background estimates and integrated luminosity for the measurement (Fig. 12(c)). Fig. 12(d) shows that the $\psi(3770)$ and the energy regions of the $\psi(4040)$ and $\psi(4160)$ exhibit small and consistent levels of $\pi\pi J/\psi$, while there is strong evidence of excess production at 4260 MeV. The data provide confirmation (11σ) of $Y(4260) \rightarrow \pi^+\pi^-J/\psi$, a first observation (5.1σ) of $Y(4260) \rightarrow \pi^0\pi^0J/\psi$ at about half the charged rate, and first evidence (3.7σ) for $Y(4260) \rightarrow K^+K^-J/\psi$. These results tend to disfavor conventional charmonium interpretations [16] and $\chi_{c\rho^0}$ molecular states [17], while being compatible with hybrid charmonium and tetraquark interpretations. Studies of open-charm production could help clarify the situation, but it is questionable if the 13.2 pb^{-1} CLEO-c sample will be sufficient.

4. Conclusion

CLEO-c is having a major impact on the world's quantitative understanding of charm decays, with broad implications for all of flavor physics. Measurements of leptonic, semileptonic, and hadronic D decays are already more precise than previous PDG values, based on a small portion of the expected data sample. Results from the CLEO-c D_s scan, including measurements of $Y(4260)$, are bonuses beyond the original project plan. CLEO-c is scheduled to run through April 2008, with expected integrated luminosity that, while short of design, will still be sufficient to

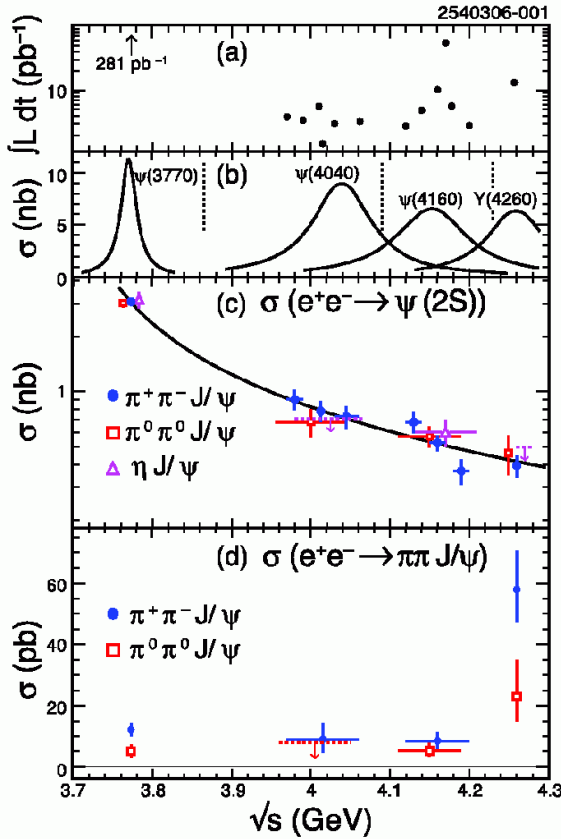


Figure 12: (a) Integrated luminosity vs. center-of-mass energy for the scan. (b) Born-level Breit-Wigner cross sections for recognized charmonium states (true cross sections) and $Y(4260)$ (arbitrary scale). (c) $e^+e^- \rightarrow \gamma\psi(2S)$ cross-section measurement vs. energy for $\pi^+\pi^-J/\psi$ (circles), $\pi^0\pi^0J/\psi$ (squares, dashed lines) and $\eta J/\psi$ (triangles) overlaid with theoretical prediction. (d) Cross sections for $e^+e^- \rightarrow \pi^+\pi^-J/\psi$ (circles) and $e^+e^- \rightarrow \pi^0\pi^0J/\psi$ (squares, dashed lines) vs. energy. Some points in (c) and (d) are offset by 10 MeV for clarity.

realize most of the program's goals: $\sim 750 \text{ pb}^{-1}$ each at $\psi(3770)$ for D physics and at 4170 MeV for D_s (and D) physics. In addition, there will be a sample of at least 30 million $\psi(2S)$ for charmonium physics. The final products will include branching fractions for $D^0 \rightarrow K^-\pi^+$, $D^+ \rightarrow K^-\pi^+\pi^+$, and $D_s^+ \rightarrow \phi\pi^+$ with precisions of $\pm 1.25\%$, $\pm 1.4\%$, and $\pm 4\%$, respectively. The ultimate precision for both D and D_s leptonic-decay branching fractions will be less than 9%. These decay-constant measurements, detailed results on semileptonic decays, including form factors, and other high-precision measurements should provide the promised and much-needed tests of LQCD and other implementations of strong-interaction theory.

Acknowledgments

I gratefully acknowledge the CESR accelerator staff for their continuing efforts to provide CLEO-c with

excellent luminosity and running conditions. CLEO-c enjoys generous support from the U.S. National Science Foundation and Department of Energy, and the Natural Sciences and Engineering Research Council of Canada. Personal communications with numerous experimental and theoretical colleagues, especially M. Voloshin, are much appreciated.

References

- [1] R. A. Briere *et al.*, Cornell University preprint CLNS-01-1742 (unpublished).
- [2] M. Artuso *et al.* [CLEO Collaboration], Phys. Rev. Lett. **95**, 251801 (2005) [arXiv:hep-ex/0508057].
- [3] C. Aubin *et al.*, Phys. Rev. Lett. **95**, 122002 (2005) [arXiv:hep-lat/0506030].
- [4] P. Rubin [CLEO Collaboration], arXiv:hep-ex/0604043.
- [5] J. L. Rosner *et al.* [CLEO Collaboration], Phys. Rev. Lett. **96**, 121801 (2006) [arXiv:hep-ex/0601027].
- [6] N. E. Adam *et al.* [CLEO Collaboration], arXiv:hep-ex/0604044.
- [7] S. Eidelman *et al.*, Phys. Lett. B **592**, 1 (2004).
- [8] G. S. Huang *et al.* [CLEO Collaboration], Phys. Rev. Lett. **95**, 181801 (2005) [arXiv:hep-ex/0506053].
- [9] T. E. Coan *et al.* [CLEO Collaboration], Phys. Rev. Lett. **95**, 181802 (2005) [arXiv:hep-ex/0506052].
- [10] J. D. Richman and P. R. Burchat *Rev. Mod. Phys.* **67**, 893 (1995)
- [11] D. Becirevic and A. B. Kaidelov, *Phys. Lett.* **B478**, 417 (2000).
- [12] C. Aubin *et al.* [Fermilab Lattice Collaboration], Phys. Rev. Lett. **94**, 011601 (2005) [arXiv:hep-ph/0408306].
- [13] M. B. Voloshin, arXiv:hep-ph/0602233.
- [14] B. Aubert *et al.* [BABAR Collaboration], Phys. Rev. Lett. **95**, 142001 (2005) [arXiv:hep-ex/0506081].
- [15] T. E. Coan *et al.* [CLEO Collaboration], Phys. Rev. Lett. **96**, 162003 (2006) [arXiv:hep-ex/0602034].
- [16] F. J. Llanes-Estrada, Phys. Rev. D **72**, 031503 (2005) [arXiv:hep-ph/0507035].
- [17] X. Liu, X. Q. Zeng and X. Q. Li, Phys. Rev. D **72**, 054023 (2005) [arXiv:hep-ph/0507177].